

AN INVERSE ANALYSIS OF UNOBSERVED TRIGGER FACTOR ACCORDING TO SLOPE FAILURE TYPES

Hirohito KOJIMA^{a,*} and Shigeyuki OBAYASHI^b

^a Dept. of Civil Engineering, Tokyo University of Science (TUS), 2641 Yamazaki Noda-City, 278-8510 JAPAN
kojima_h@rs.noda.tus.ac.jp

^b Applied laboratory of spatial Information, 2-5-20 Muromachi, Sakaiide-City, 150-0036 JAPAN

KEY WORDS: Slope failure types, Trigger factors, Inverse analysis, Structural equation modeling, Spatial data integration

ABSTRACT:

This paper discusses an inverse analysis of unobserved trigger factors according to “slope failure types” based on Structural Equation Modeling (SEM). Quantitative prediction models generally elucidate the relationship between past slope failures and causal factors (e.g., geology, topography, soil, slope, aspect, drainage, land cover, etc.), but do not consider trigger factors (e.g., rail fall, earthquake, weathering, etc.), due to difficulties in pixel-by-pixel observations of trigger factors. As one of the measures, an inverse analysis algorithm on trigger factor has been proposed according to the following steps:

- **Step 1:** The relationship between past slope failures (i.e., the endogenous variables), causal and trigger factors (i.e. the exogenous variables) are delineated on the path diagram used in SEM approach,
- **Step 2:** The regression weights in the path diagram are estimated based on the maximum likelihood estimation procedure; and
- **Step 3:** Through the “measurement equation” defined between the causal factors (i.e., observed variables) and the trigger factor (i.e., unobserved latent variable), the trigger factor is inversely estimated, and a trigger factor influence (TFI) map is also produced. As a subsequent subject from previous study, the TFI maps are produced with respect to “different types” of slope failures which are “surface failure,” “deep-seated slope failures,” and “landslides,” separately. As a final outcome, the differences in these TFI maps are delineated on a “difference (DIF) map.” These DIF maps enable us to analyze the difference of trigger factor influence with respect to slope failure types simultaneously. Such “heuristic information” would be useful for assessing the hazardous area with respect to the different types of slope failures, as well as for improving the cost-effectiveness in locating various slope measuring systems (e.g., the tensiometer, the rain gauge, etc.).

1. INTRODUCTION

Due to the limitation of detail field investigation, spatial data integration approaches applying the satellite remotely sensed data and the various kinds of geographical information (termed “causal factor”) are highly expected for identifying the hazardous area affected by the slope failures. Slope stability evaluation models have generally constructed the relationship between the past occurrences of slope failures and the causal factors (Chung et al., 1999; Crozier et al., 2002; Obayashi et al., 1999), but have not dealt with the trigger factors (e.g., rainfalls, earthquakes, weathering, etc.), due to the difficulties of obtaining pixel-based observations on those triggering factors (Carrara et al., 1998).

As another viewpoint on the previous research works, we regarded the trigger factors as “unobserved factors” rather than “observed factors” in terms of time and space. Based on this concept, we have constructed a Trigger Factor Inverse-analysis algorithm (termed the “TFI algorithm (Kojima et al., 2006)”) for the slope failures by the SEM (Structural Equation Modeling) approach. In the TFI algorithm, pixels corresponding to the past slope failures are generally used as the input data of endogenous variables (i.e., training data sets). The estimated values of the trigger factor are delineated on the Trigger Factor Influence map (termed “TFI map”), which depends on the distribution of past slope failures used as the training data sets.

With those research activities as background, one of the subsequent requirements for slope failure hazard mapping is to estimate the influences of trigger factors according to slope

failure types. To overcome this difficulty, our efforts in this study are to:

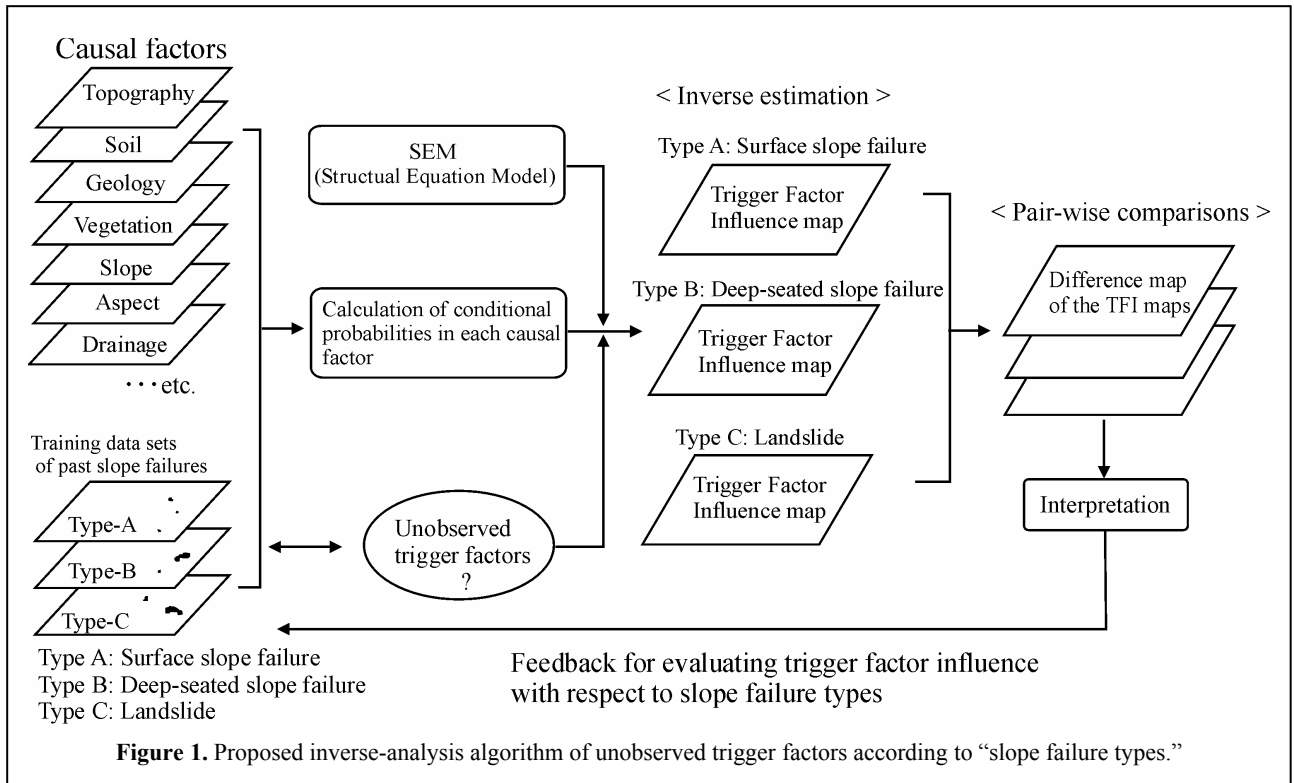
- construct the inverse analysis procedure of unobserved trigger factor for the “different types of slope failures”; and
- produce the Trigger Factor Influence maps (TFI map) according to different types of slope failures, as well as to consider those applications for the slope failure hazard assessments.

2. STUDY AREA AND QUANTITATIVE MODEL

2.1 Study Area and Spatial Input Data Sets

The study area is located on Yamakoshi-mura in Niigata prefecture, Japan, where the various types of slope failures had caused by the huge earthquake on October 23, 2004, following the local-downpour on July 13, 2004. Through the field investigation with the aerial photographs, those occurrences were precisely plotted on the topographical map as the training data sets for constructing the quantitative prediction model.

The quantitative prediction model constructed the relationship between the past occurrences of slope failures and the following nine “causal factors”: (1) Soil, (2) Surface geology, (3) Topography, (4) Vegetation index, (5) Slope, (6) Aspect, (7) Drainage, (8) Elevation, and (9) Relief. Each map consists of 120 × 100 pixels (3.6 Km × 3.0 Km, 30m/pixels) corresponding to the ground resolution of the IKONOS data). The latter five factors were produced based on the Digital Terrain Model



(DTM). The experts in each research field have made Soil-, Surface geology- and Topographical- map. The vegetation index map is also produced by calculating the Normalized Vegetation Index (NVI) given by

$$NVI = (B4 - B3) / (B4 + B3) \quad (1)$$

where $B3$ and $B4$ are the digital numbers in each pixel corresponding to IKONOS Bands 3 and 4, respectively.

2.2 Quantitative Prediction Models

Figure 1 shows the proposed inverse-analysis algorithm of the trigger factors according to slope failure types, expanding the previous quantitative prediction model (Kojima et al., 2006). Chung and Fabbri (1999) have adopted the formulas for geologic hazard zonation as a part of "favorability function" approaches. To promote those prediction models as well as optimizing prediction, we had proposed the following analytical procedures:

- Comparative strategy of the prediction models (Kojima et al., 1998; Obayashi et al., 1999);
- Analysis of the landslide types (Kojima et al., 2000);
- Testing on the time-robustness in prediction (Kojima et al., 2001); and
- Sensitivity analysis of the prediction models with respect to the causal factors (Chung et al., 2002).

These analytical procedures are crucial components in the prediction models, and are indeed useful for not only the experts working on the slope failure hazard assessments, but also the end-users of the prediction models. However, the conventional prediction models generally construct the relationship between the past slope failures and the causal factors, but do not apply the trigger factors, because of the difficulties in pixel-by-pixel observations of trigger factors.

As a measure against these difficulties, an inverse analysis algorithm on unobserved trigger factor had been presented (Kojima et al., 2006), based on the Structural Equation Modeling

(SEM). SEM is also well known as the “analysis of covariance structures,” in a word, SEM can be regarded as a model integrated the regression analysis jointly with the exploratory factor analysis. The detail of SEM itself is available for the references (Hoyle et al., 1995).

3. INVERSE ANALYSIS OF TRIGGER FACTOR

The proposed algorithm for inverse analysis of trigger factors according to slope failure types (see **Figure 1**) consists of the following steps:

3.1 Description of Input Data

To construct a probability model for slope failure hazard, consider the following proposition:

F_p : “a pixel p will be affected by a future slope failure of a given type X .”

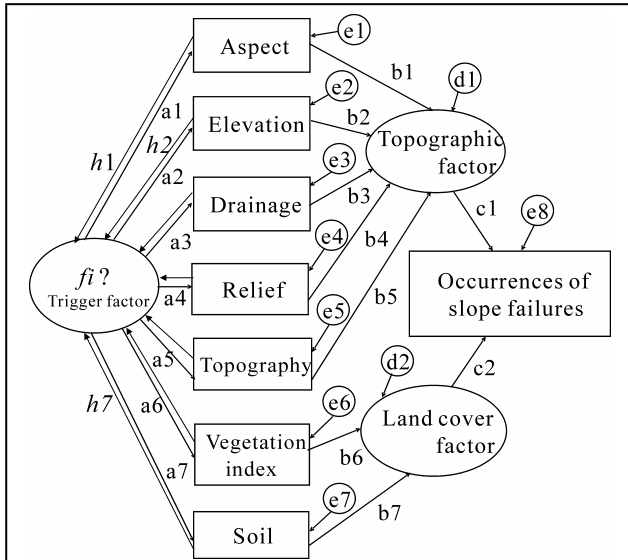
The conditional probabilities in each causal factor given by

$$\mathbf{Prob}(F_p | C_{ij}) = T_{ij} / N_{ij} \quad (2)$$

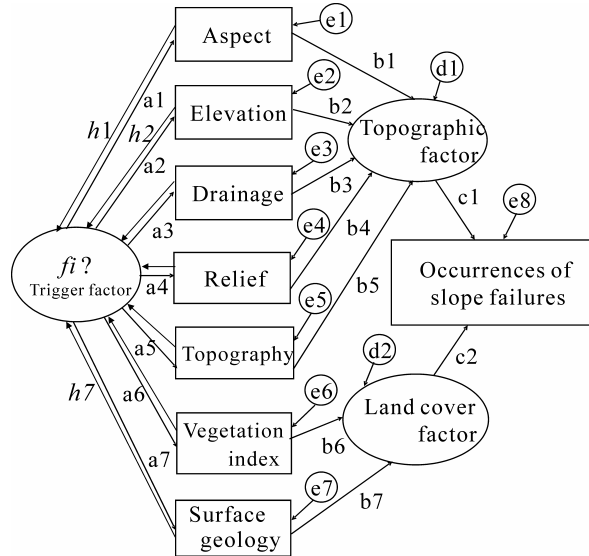
where C_{ij} is the i^{th} category of the j^{th} causal factor; N_{ij} is the number of pixels of C_{ij} ; and T_{ij} is number of pixels of the past slope failures that had occurred in the area corresponding to C_{ij} . $\mathbf{Prob}(F_p | C_{ij})$ are used as the input data for the SEM-based analysis.

3.2 Path Diagrams

To construct a quantitative prediction model, the relationship between the past slope failures (i.e., endogenous variables), the causal and trigger factors (i.e., exogenous variables) should be delineated on the path diagram used in the SEM. Let us consider the path diagram as shown in **Figure 2** that is called a recursive mode (Kojima et al., 2006). $\mathbf{Prob}(F_p | C_{ij})$ of **Equation 2** are the input data as the exogenous variables, while the pixels



(a) Model A: using training data set with respect to “surface slope failure”



⊙ : error variable □ : observed variable
 ⊙ : disturbance variable ○ : unobserved variable
 a,b,c : regression variable

(b) Model B and Model C: using training data sets with respect to “deep-seated slope failure” and “landslide,” respectively.

Figure 2. Path diagrams for SEM-based analysis.

corresponding to occurrences and non-occurrences of the slope failures are assigned to the value “1” or “0”, respectively, that are used as the endogenous variables. To exclude a multicollinearity between causal factors, among a pair of causal factors with high correlation (e.g., above 0.7), one of a pair with high partial correlation was selected. **Figures 2a** and **2b** shows the path diagrams composed of selected causal factors. The training data sets (i.e., endogenous variables) of these models are as follows:

- Model A: using training data sets of “surface slope failure”;
- Model B: using training data sets of “deep-seated slope failure”; and

Table 1. Evaluating model fit.

Measure of fit	Model A	Model B	Model C
GFI	0.995	0.991	0.997
AGFI	0.988	0.976	0.992
AIC	280.0	423.9	208.0
RMSEA	0.036	0.051	0.029

Notes:

GFI: Goodness of Fit Index,
 AGFI: Adjusted Goodness of Fit Index,
 AIC: Akaike Information Criterion; and
 RMSEA: Root Mean Square Error Approximation

- Model C: using training data sets of “landslide.”

3.3 Evaluating Model Fit

Not knowing the trigger factors, the program is how to estimate the regression weights in the path diagrams of $\{a_1, \dots, a_n, b_1, \dots, b_n, c_1, \dots, c_n\}$ shown in **Figure 2**. These weights are estimated to minimize errors between the observed- and estimated- “variance-covariance matrix” by the model. Among various estimation procedures (e.g., maximum likelihood estimation, asymptotically distribution-free estimation, generalized least squares estimation, “scale free” least squares estimation, unweighted least squares estimation, etc.), for this study, the maximum likelihood (ML) estimation procedure was selected, which is generally reported as a better estimator for the large population.

For evaluating model fit, the Goodness of Fit Index (GFI), the Adjusted Goodness of Fit Index (AGFI), the Akaike Information Criterion (AIC), and the Root Mean Square Error Approximation (RMSEA) are applied as the generally employed statistical measures of fit. Details on these fit measurements are available in Hoyle(1995). **Table 1** shows the results of these fit measures.

By rule of thumb, GIF and AGFI need to be more than 0.9, conversely, RMSE should be less than 0.08 for selecting reasonable model. AIC are also used to “comparison” of the model fit. The model with lower value of AIC is considered to have better fit from the other. Based on these criterions, **Table 1** gives us an indication of which all models can be accepted to the following analysis.

3.4 Inverse Analysis of Trigger Factor

Note that the path components connecting unobserved variables to each other and observed variables to unobserved variables are generally termed “structural equations” and “measurement equations,” respectively. In this study, through the measurement equation, the influence of trigger factor is inversely estimated in each pixel. The estimated values are also delineated on a TFI map. In the path diagram shown in **Figure 2**, the measurement equation between trigger factor (i.e., unobserved variables) and causal factors (i.e., observed variables) is given by:

$$z_{ji} = a_j f_i + e_{ji} \quad (3)$$

where Z_{ji} is the input value of the i^{th} pixel in the j^{th} causal factor as shown in **Equation 2**; a_j is the path parameter linking the j^{th} causal factor with the trigger factor; f_i is the unobserved

trigger factor (see **Figure 2**) in the i^{th} pixel; and e_{ji} is the error term of the i^{th} pixel in the j^{th} causal factor. The average and variance for z_{ji} and f_i are standardized to 0 and 1, respectively.

The objective is to inversely calculate the estimates for f_i of the trigger factor. Suppose \hat{f}_i is the estimate of f_i , then, the inverse function is given by:

$$\hat{f}_i = \sum_{j=1}^p h_j z_{ji} \quad (4)$$

where p is the number of causal factors. Parameters of $\{h_1, h_2, \dots, h_p\}$ are determined by minimizing the following square error:

$$Q = \sum_{i=1}^n (f_i - \hat{f}_i)^2 = \sum_{i=1}^n (f_i - \sum_{j=1}^p h_j z_{ji})^2 \rightarrow \text{minimizing}$$

$$\frac{\partial Q}{\partial h_j} = -2 \sum_{i=1}^n z_{ji} (f_i - \sum_{j=1}^p h_j z_{ji}) = 0 \quad (5)$$

Hence, $\{h_1, h_2, \dots, h_p\}$ are simply given by:

$$h_j = \sum_{j'=1}^p a_{j'} r^{jj'} \quad (6)$$

where $r^{jj'}$ is the element (j, j') of the inverse matrix for the correlation matrix between causal factors. Using **Equation 4**, \hat{f}_i can be calculated in each pixel and is delineated on the TFI map proposed in this study.

Figure 3 indicates the Trigger Factor Influence (TFI) maps with respect to slope failure types of “surface slope failure,” “deep-seated slope failure,” and “landslide,” respectively. The estimated patterns between these TFI maps according to the slope failure types are obviously different. The pixels with higher estimated value, for the landslide type and the deep-seated slope failure type, are almost distributed in the central and the east part in the study area, respectively.

These results suggest that trigger factor influences with respect to the types of slope failures would be different, and trigger factor can be inversely estimated pixel-by-pixel through the path model shown in **Figure 2**. For supporting better interpretation of trigger factor influences, let us consider the pair-wise comparison of these TFI maps in the next section.

4. EVALUATION OF TRIGGER FACTOR INFLUENCE

4.1 Success Rate

To evaluate the performance of model itself, the “success rates” are calculated as shown in **Figure 4**. 10% of X axis means the pixels with the highest 10% estimated values on the trigger factor influence are classified as hazardous. Among these pixels, the rate of correctly classifying the pixels of slope failures, used as the training data, is indicated on Y axis as “success rate.” Also, for the pixels with the highest $\{20\%, 30\%, \dots, 90\%\}$ of estimated values, the success rates were calculated repeatedly.

If the model is “reasonably good,” then one would expect that the success rate of the corresponding first class with 10 % estimated value, which is defined as hazardous area, should be much higher than 10%. For the pixels with the highest 30% of estimated value, **Figure 3** indicates that the success rates on all slope failure types are more than 80%, which means the inverse

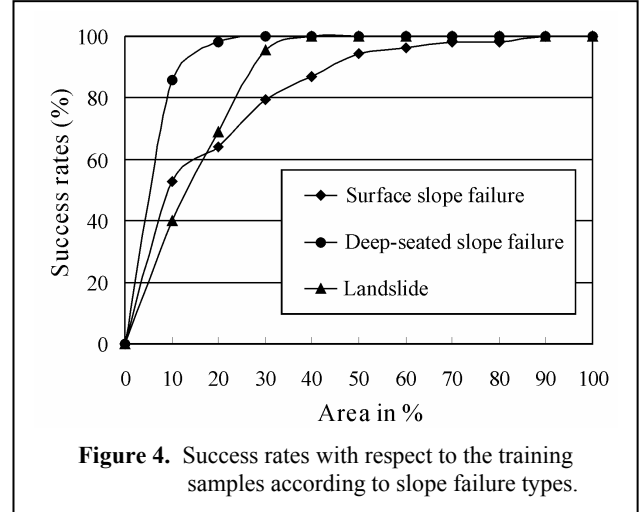


Figure 4. Success rates with respect to the training samples according to slope failure types.

analysis approach would be applicable for evaluating the trigger factor influence with respect to the slope failure types.

4.2 Matching Rate

In order to evaluate the difference of trigger factor influence according to the slope failure types, the matching rates, as shown in **Figure 5**, are also calculated with the same calculation procedure of success rates. The matching rates are defined as the correct classified ratio of pixels on trigger factor influence maps to the past slope failures used as the training data sets. The comparative cases for calculating matching rates are as follows:

- Case 1: TFI map on “surface slope failure” vs. training data of “deep-seated slope failure,”
- Case 2: TFI map on “surface slope failure” vs. training data of “landslide,”
- Case 3: TFI map on “deep-seated slope failure” vs. training data of “surface slope failure,”
- Case 4: TFI map on “deep-seated slope failure” vs. training data of “landslide,”
- Case 5: TFI map on “landslide” vs. training data “surface slope failure”; and
- Case 6: TFI map on “landslide” vs. training data of “deep-seated slope failure.”

Figure 5b gives us an indication of which the highest position of matching rate curve comes from Case 3, but not so high. As a whole, the matching rates of all comparative cases indicate low values. Especially, the matching rate curve of Case 6 is at the lowest position. These results suggest that the trigger factor influences according to slope failure types would be different in this study area, and the proposed inverse model has higher sensitivity for evaluating trigger factors with respect to “slope failure types” as well.

4.3 Difference Map

To clarify the difference of trigger factor influence, the difference maps (termed DIF map) with all combination cases of TFI maps are produced as shown in **Figure 6**. Note that the legend for **Figure 6** leads to the following interpretation on the difference of trigger factor influence:

- Shade of red: The degree of trigger factor influence for Type A of slope failure is higher than that of Type B.
- White: The degree of trigger factor influence for Type A of slope failure is almost equivalent to that of Type B.

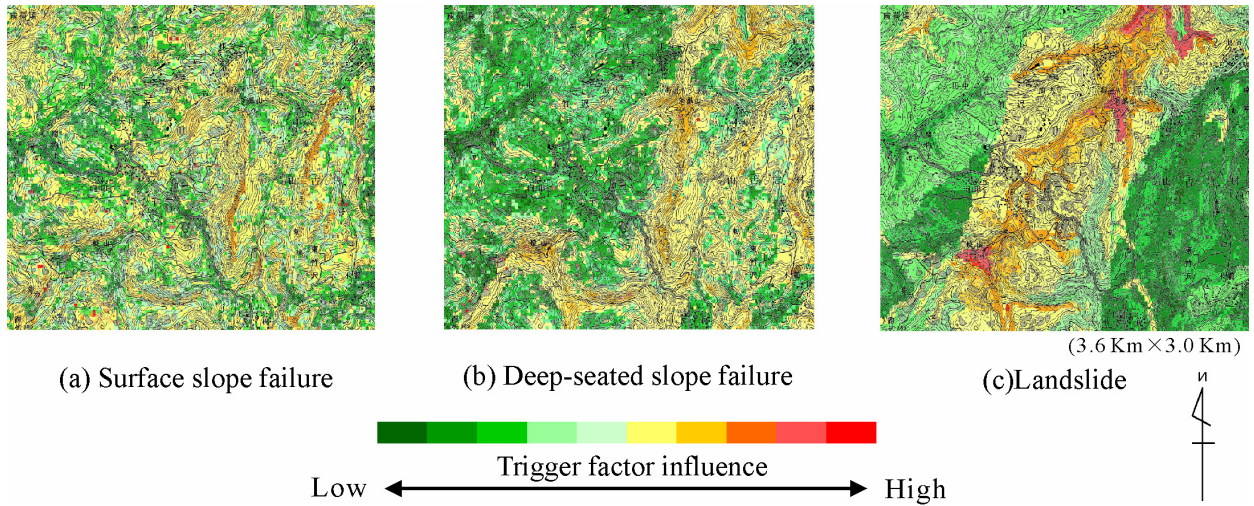
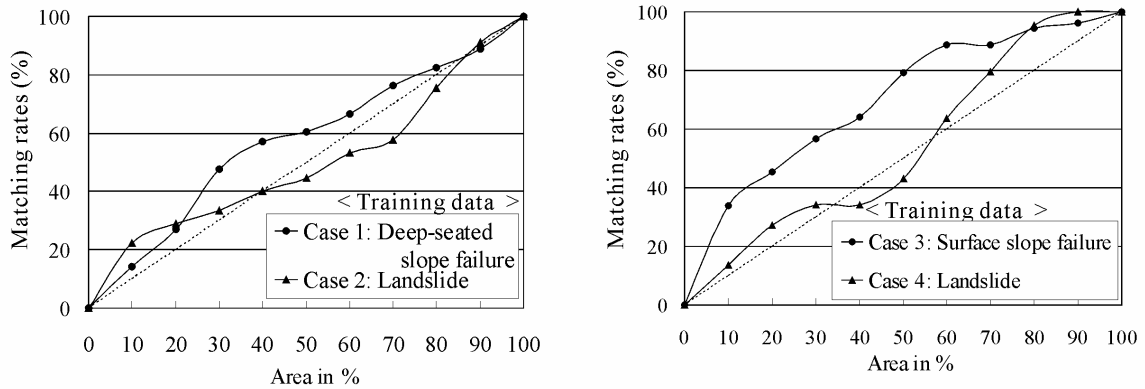
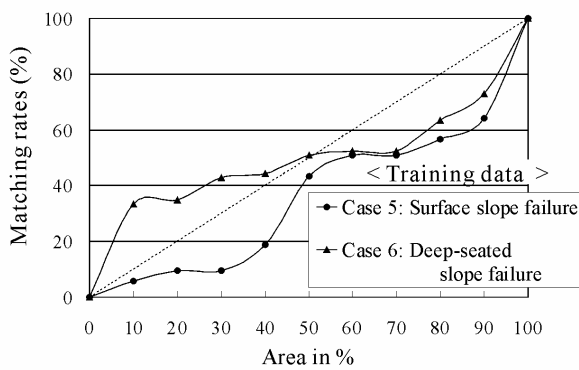


Figure 3. Trigger factor influence maps according to slope failure types.



(a) TFI map on "Surface slope failure" vs. Training data sets of "Case 1 and Case 2."

(b) TFI map on "Deep-seated slope failure" vs. Training data sets of "Case 3 and Case 4."



(c) TFI map on "landslide" vs. Training data sets of "Case 5 and Case 6."

- Notes: The comparative cases for calculating "matching rates" are as follows:
- Case 1: TFI map on "surface slope failure" vs. training data of "deep-seated slope failure,"
 - Case 2: TFI map on "surface slope failure" vs. training data of "landslide,"
 - Case 3: TFI map on "deep-seated slope failure" vs. training data of "surface slope failure,"
 - Case 4: TFI map on "deep-seated slope failure" vs. training data of "landslide,"
 - Case 5: TFI map on "landslide" vs. training data "surface slope failure"; and
 - Case 6: TFI map on "landslide" vs. training data of "deep-seated slope failure."

Figure 5. Matching rates between trigger factor influence maps and training data sets according to slope failure types.

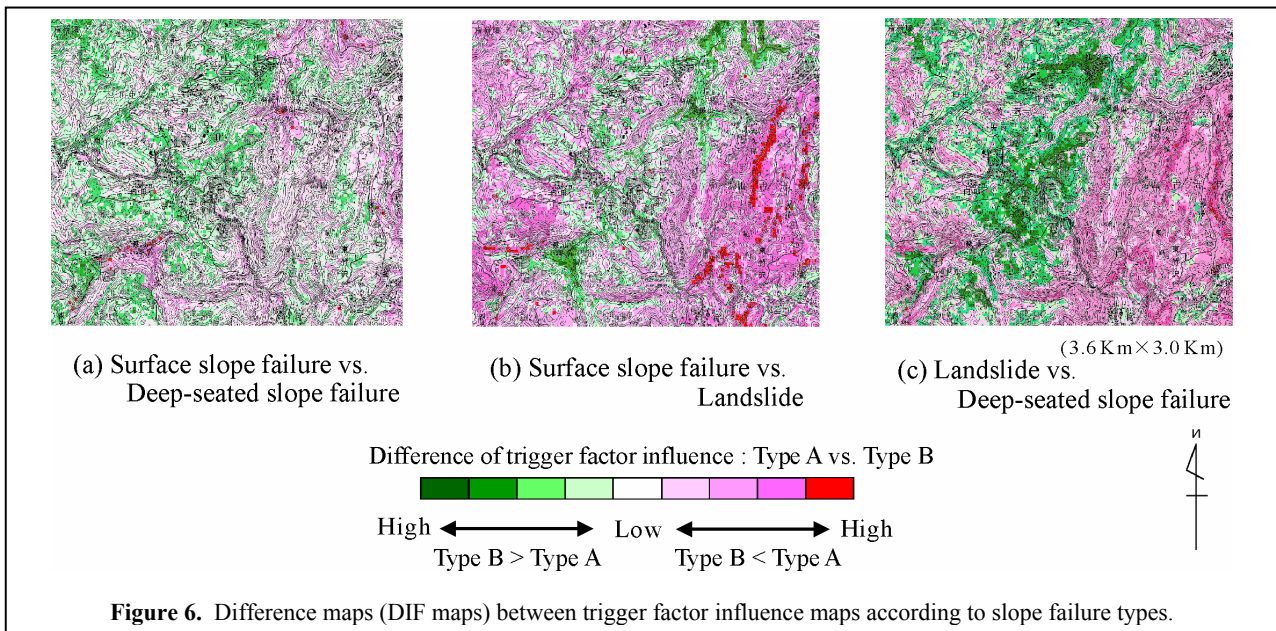
- Shade of green: The degree of trigger factor influence for Type A of slope failure is lower than that of Type B.

The difference maps enable us to analyze the differences of trigger factor influences with respect to slope failure types simultaneously. Such visualization strategy with "heuristic information" would be useful for assessing the hazardous area with respect to the different types of slope failures, as well as for improving the cost-effectiveness in locating various slope measuring systems (e.g., the tensiometer, the rain gage, etc.)

5. CONCLUDING REMARKS

In this contribution, we have discussed about an inverse analysis of the unobserved trigger factor according to the slope failure types, based on the SEM approach. The results of this study can be summarized as follows:

- Due to the difficulties of pixel-based observations of the slope failure trigger factors, we have strongly pointed out the



necessity for the inverse estimation of “unobserved trigger factor.” As a measure, through the measurement equation defined between the causal factors (i.e., observed variables) and trigger factors (i.e., unobserved variables), a “Trigger Factor Influence map (TFI map)” was produced.

- As an application of the proposed algorithm of inverse analysis, the TFI maps were produced according to the different types of slope failure, separately. As a final outcome, the differences of these TFI maps was delineated on a “Difference map (DIF map).”
- Through the DIF maps, we can evolve the analysis on the “trigger factor influence” with respect to the slope failure types, jointly with the expert's opinions.

This study was executed for the earthquake-induced slope failures in Niigata prefecture. For future work, to corroborate the practicality of the inverse analysis algorithm (Figure 1), the rainfall-induced trigger factor should be considered. From this point of view, the analytical procedure shown in Figure 1 can be adopted as a standard approach for slope failure hazard assessment. As regards the structure of path diagram in Figure 2, a “single” exogenous variable is considered as the trigger factor. However, in practice, either slope failures or landslides are caused by various trigger factors, so that modified path model with several exogenous variables as trigger factors should be investigated to improve identification of the model itself.

Note that the precise estimation of trigger factor on the slope failure is impossible. As one of the measures, the inverse analysis algorithm presented in this study, as well as “heuristic information” on the DIF maps between the TFI maps would be effective for identifying the hazardous area affected by “different types” of slope failures. Such a systematic analytical procedure would be essential to overcome some of the limitations of conventional approaches in prediction modeling for the slope failure hazard mapping.

ACKNOWLEDGEMENTS

Funding was partly supported by the “Grant-in-Aid for Scientific Research Program (No.19651079)” of the Ministry of Education, Culture, Sports, Science and Technology (MEXT) in Japan.

REFERENCES

- Carrara, A., 1998. Current limitations in modeling landslide hazard, *Proceedings of The International Association for Mathematical Geology*, No.4, pp.195-203.
- Crozier, M.J., and T.Glade, 2002. Landslide hazard and risk, Issues, Concepts and Approach, *Landslide Hazard and Risk*, John Wiley & Sons Publication, pp.22-24.
- Chung, C.F., and A.G. Fabbri, 1999. Probabilistic prediction models for landslide hazard mapping, *Photogrammetric Engineering & Remote Sensing*, Vol.65, No.12, pp.1389-1399.
- Chung, C.F., H. Kojima, and A.G. Fabbri, 2002. Applied Geomorphology: theory and practice, Stability analysis of prediction models applied to landslide hazard mapping, *John Wiley & Sons Publication*, pp.3-19.
- Hoyle, R.H., 1995. Structural equation modeling approach: Basic concepts, and fundamental issues. In: *Hoyle, R.H., (Eds.), Structural Equation Modeling: Concepts, Issues, and Applications*, Sage publications, pp.1-15.
- Kojima, H., C.F. Chung, S. Obayashi, and A.G. Fabbri, 1998. Comparison of strategies in prediction modeling of landslide hazard zonation, *Proceedings of The International Association for Mathematical Geology*, No.4, pp.195-203.
- Kojima, H., C.F. Chung, and C.J. van Westin, 2000. Strategy on the landslide type analysis based on the expert knowledge and the quantitative prediction model, *International Archives of Photogrammetry & Remote Sensing*, Vol.33, Part-B7, pp.701-708.
- Kojima, H., and C.F. Chung, 2001. Testing on the time-robustness of a landslide prediction model, *Proceedings of The International Association for Mathematical Geology*, Vol.7, pp.41-46.
- Kojima, H., and S. Obayashi, 2006. An inverse analysis of unobserved trigger factor for slope stability evaluation, *Computers & Geosciences*, Vol.32, Issue 8, pp.1069-1078.
- Obayashi, S., H. Kojima, and C.F. Chung, 1999. Comparison of the accuracy of the slope stability evaluation models and its practical application, *Journal of the Construction Management and Engineering, Japan Society of Civil Engineers (in Japanese)*, No.630, 6-44, pp.77-89.